AD_____

GRANT NUMBER: DAMD17-94-J-4424

TITLE: Single-Pulse Dual-Energy Mammography Using a Binary
Screen Coupled to Dual CCD Cameras

PRINCIPAL INVESTIGATOR: John M. Boone, Ph.D.

CONTRACTING ORGANIZATION: University of California
Davis, CA 95616

REPORT DATE: August 1996

TYPE OF REPORT: Annual

DTIC QUALITY INSPECTED 2

PREPARED FOR: Commander
U.S. Army Medical Research and Materiel Command
Fort Detrick, Frederick, MD 21702-5012

DISTRIBUTION STATEMENT: Approved for public release;
distribution unlimited

The views, opinions and/or findings contained in this report are
those of the author(s) and should not be construed as an official
Department of the Army position, policy or decision unless so
designated by other documentation.

19961021 085

DISCLAIMER NOTICE
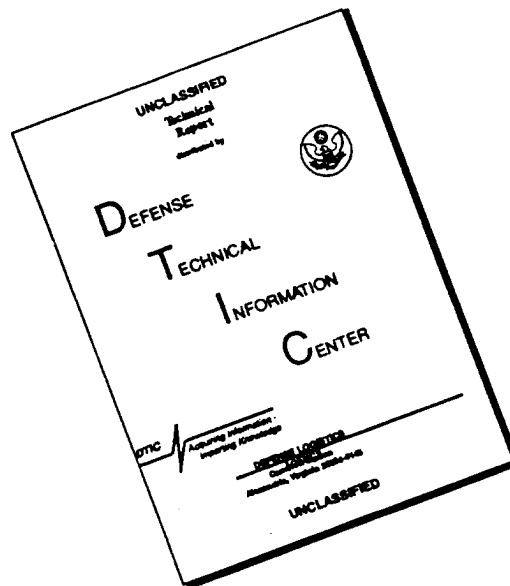
THIS DOCUMENT IS BEST QUALITY AVAILABLE. THE COPY FURNISHED TO DTIC CONTAINED A SIGNIFICANT NUMBER OF PAGES WHICH DO NOT REPRODUCE LEGIBLY.

REPORT DOCUMENTATION PAGE

Form Approved
OMB No. 0704-0188

1. AGENCY USE ONLY *(Leave blank)*	2. REPORT DATE August 1996	3. REPORT TYPE AND DATES COVERED Annual (15 Jul 95 - 14 Jul 96)

4. TITLE AND SUBTITLE
Single-Pulse Dual-Energy Mammography Using a Binary
Screen Coupled to Dual CCE Cameras

5. FUNDING NUMBERS
DAMD17-94-J-4424

6. AUTHOR(S)
John M. Boone, Ph.D.

7. PERFORMING ORGANIZATION NAME(S) AND ADDRESS(ES)
University of California
Davis, CA 95616

8. PERFORMING ORGANIZATION REPORT NUMBER

9. SPONSORING/MONITORING AGENCY NAME(S) AND ADDRESS(ES)
Commander
U.S. Army Medical Research and Materiel Command
Fort Detrick, MD 21702-5012

10. SPONSORING/MONITORING AGENCY REPORT NUMBER

11. SUPPLEMENTARY NOTES

12a. DISTRIBUTION / AVAILABILITY STATEMENT
Approved for public release; distribution unlimited

12b. DISTRIBUTION CODE

13. ABSTRACT *(Maximum 200)*

This past year we have been working on a wide variety of different research topics, where each relates to the global objective of this proposal but the individual projects are only loosely related to each other. The projects that are reported here are (1) x-ray spectral measurements, (2) novel screen evaluation, (3) analytical screen comparisons, (4) evaluation of attenuation coefficient data, (5) the development of a sine wave test pattern approach to measuring the MTF, (6) development of an image registration algorithm, (7) calculation of breast density from digital mammograms, and (8) mechanical fabrication of the digital mammography system.

Progress in each of these projects has been substantial, and five manuscripts have been or will be shortly submitted covering these topics. Here we report, in vignette format, representative examples of the results of each of the projects. With these parallel efforts completed or close to completion (depending on which project) and the groundwork laid, in the upcoming year we can turn our focus towards putting together the actual dual energy mammography system, testing it, and evaluating its potential. We look forward to these continuing efforts with enthusiasm and optimism that dual energy mammography may be a realistic tool in the diagnostic work-up for breast cancer.

14. SUBJECT TERMS		15. NUMBER OF PAGES 27
Breast Cancer Detection	Dual Energy Digital Mammography	16. PRICE CODE

17. SECURITY CLASSIFICATION OF REPORT	18. SECURITY CLASSIFICATION OF THIS PAGE	19. SECURITY CLASSIFICATION OF ABSTRACT	20. LIMITATION OF ABSTRACT
Unclassified	Unclassified	Unclassified	Unlimited

FOREWORD

Opinions, interpretations, conclusions and recommendations are those of the author and are not necessarily endorsed by the US Army.

_____ Where copyrighted material is quoted, permission has been obtained to use such material.

_____ Where material from documents designated for limited distribution is quoted, permission has been obtained to use the material.

__✓__ Citations of commercial organizations and trade names in this report do not constitute an official Department of Army endorsement or approval of the products or services of these organizations.
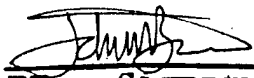
_____ In conducting research using animals, the investigator(s) adhered to the "Guide for the Care and Use of Laboratory Animals," prepared by the Committee on Care and Use of Laboratory Animals of the Institute of Laboratory Resources, National Research Council (NIH Publication No. 86-23, Revised 1985).

__✓__ For the protection of human subjects, the investigator(s) adhered to policies of applicable Federal Law 45 CFR 46.

_____ In conducting research utilizing recombinant DNA technology, the investigator(s) adhered to current guidelines promulgated by the National Institutes of Health.

_____ In the conduct of research utilizing recombinant DNA, the investigator(s) adhered to the NIH Guidelines for Research Involving Recombinant DNA Molecules.

_____ In the conduct of research involving hazardous organisms, the investigator(s) adhered to the CDC-NIH Guide for Biosafety in Microbiological and Biomedical Laboratories.

5 August 1996
PI - Signature   Date

iii

4. Table of Contents

Single-Pulse Dual-Energy Mammography using a binary screen coupled to dual CCD cameras

---

5. Introduction

5.1 Background

Breast Cancer and Mammography

Breast cancer will strike approximately one in nine women in the United States, making it the most common form of cancer amongst women. In 1992, there were over 46,000 deaths due to breast cancer and 180,000 new cases were detected. Presently, there is no cure for this devastating disease and the best hope for patients stricken with breast cancer lay in its early detection. While ultrasound and MRI are modalities that have been aimed at the breast, x-ray mammography has the best sensitivity for the early detection of breast cancer in women who are asymptomatic. Hence, screen film mammography has proliferated substantially over the last 5 years as an important "front line" against breast cancer.

Mammography makes use of high resolution screen-film detector systems. The x-rays that pass through the patient's breast are detected by a thin screen composed of a phosphor which emits visible light when struck by x-rays. The visible light that is emitted by the x-ray screen phosphor is detected by the film emulsion, which is physically sandwiched with the screen. Although screen-film technology has been used in radiography for almost 100 years, the extraordinary requirements of mammography push the sensitivity, resolution, and dynamic range of screen-film systems to the limit. Dense breasts often push this technology beyond its limits.

The dense breast poses a significant problem in mammography. Although there are areas in the dense breast where x-rays penetrate relatively easily (non-dense regions near the skin line), the dense regions of the breast attenuate so many of the x-rays that only a few photons pass through the breast and strike the detector below it. Therefore, the film underlying these dense areas can be markedly underexposed. The exposure cannot be increased to accommodate this, because an overexposure of the areas of the breast that are not extremely dense would occur. X-ray tube output limitations and motion artifacts due to long exposure times further compound the problem. The problem results directly from the fact that the screen-film detector used for mammography has a limited *dynamic range*, which is also called *latitude* in radiography. This is illustrated below:

Figure 1. The dense areas of a dense breast attenuate so much of the incident x-ray fluence that the film is underexposed in these areas (indicated by "B"). The exposure cannot be increased to accommodate this problem because that would result in overexposure of other areas in the image (indicated by "A").
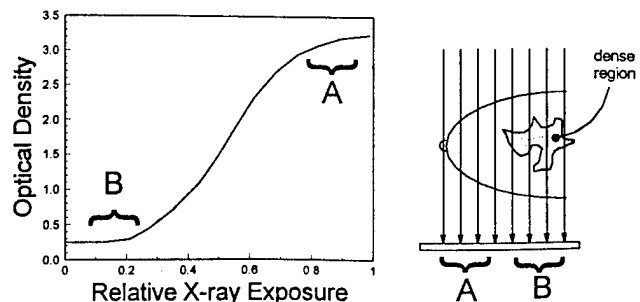
One solution to the limited dynamic range of film would be to simply increase the latitude of the film, however, a loss of radiographic contrast would be the unavoidable compromise. General Electric has recently produced a mammographic system with a rhodium target in addition to molybdenum. The rhodium generates a higher energy spectrum, which reduces subject contrast and therefore the dynamic

range requirements. However, the value of this system is yet to be fully understood in the clinical environment. Another approach to increasing the dynamic range is to make use of electronic/digital detection methods, which in most cases have substantially better dynamic range than film:

Digital Mammography

While screen-film mammography has evolved in recent years as the clinical gold standard, advances in computer detection algorithms and computer aided diagnosis in mammography have led to the hope that digital mammographic systems would become clinically and routinely available. Towards this end, the development of digital mammographic systems and their applications have been studied by several investigators. In September of 1991 the National Cancer Institute sponsored a workshop entitled: "Breast imaging: state of the art and technologies of the future". The consensus of this workshop was that digital mammography was considered, "...the most fertile territory for major advances in the x-ray detection and diagnosis of minimal breast cancers".[1] Recently (August 1992) in Calgary, Dr. Faina Shtern of the Diagnostic Imaging Research Branch, Division of Cancer Treatment at the National Cancer Institute underscored the significance of digital mammography in the diagnosis of breast cancer[1].

The success of digital mammography in breast cancer detection will require development in two general areas: (1) computer analysis techniques which use mammograms in digital format, irrespective of the digitization procedure, and (2) the development of digital mammographic acquisition hardware.

Digital Mammography, Software Applications

The applications which show promise for improving the detection of breast cancer include pattern recognition techniques for the identification of microcalcifications[2-4], soft tissue masses[5], or pathological texture[6]. Numerous studies (those referenced and many others) have indicated, at least preliminarily, that pattern recognition software may augment and improve the radiologist's detection and identification of breast cancer. Though the trained human eye is incredibly good at pattern recognition, Dr. Maryellen Giger's characterization[7] of the role of pattern recognition software in digital mammography as a "second opinion" is well-put and succinct: While it is unlikely in the short term that such software will outperform the radiologist, the combined efforts of pattern recognition software *and* the radiologist can probably outperform the radiologist alone. The research in this area has generally been pursued using conventional screen-film mammograms, digitized by a laser scanner.

Direct Digital Acquisition, Hardware Development

Digital radiography has been investigated by many researchers with many different motives. Digital mammography pushes digital acquisition techniques to their technical limits due to the high spatial resolution and low dose requirements imposed by breast imaging. One generic advantage of digital radiography is that the detector technology is divorced from the display technology, unlike in screen-film systems. By divorcing detection and display, each of those responsibilities can be assigned to dedicated equipment, and therefore the detector can be optimized for detection, and the display device

3

can be optimized for display. As mentioned before, electronic detectors also have significantly better dynamic range than conventional screen-film combinations. The whole breast can be imaged without loss of contrast in regions of too low or too high exposure, as often occurs with screen-film systems. Another excellent example where digital detectors may play an important role in cancer detection is with dual-energy mammographic acquisition. In dual-energy imaging, calcified areas of the patient can be enhanced due to the intrinsic physical properties of x-ray absorption, as opposed to pattern recognition or imaging processing enhancements. Since the breast contains no naturally occurring calcific structures (i.e. no bones) and since calcification is a very important diagnostic finding in the diagnosis of breast cancer, dual-energy imaging has great potential in mammography. Dual-energy acquisition requires the detection of two images, one at low x-ray energies and the other at a higher energies.

5.2 Statement of Work

The original statement of work is provided for reference. This report comes at the end of the second year of the four years of funding of this grant, and so Tasks 1 and 2 were to be met at this point in time.

Task 1: Computer Simulation of Dual-Energy Digital Mammography System [months 1-24]

1.1. The most efficient x-ray spectrum, which depends on the anode target material (Molybdenum or Tungsten), the kilovoltage, and the thickness and composition of the pre-patient filter, will be identified for dual energy mammography

1.2. The most efficient x-ray spectrum, which depends on the anode target material (Molybdenum or Tungsten), the kilovoltage, and the thickness and composition of the pre-patient filter, will be identified for single energy mammography

1.3. The best thickness and phosphor ratio (e.g. mg Y_2O_2S versus mg Gd_2O_2S) for dual energy mammography will be identified using computer simulation with a typical breast thickness (4.2 cm).

1.4. The most efficient anti-scatter grid ratio and construction will be identified using the figure of merit $[SNR]^2$ / [Average Glandular Dose]

Task 2: Design and Construct Dual-Energy Mammography Imaging System [months 1-24]

2.1. Consult with mechanical engineer (consultant on project) and finalize design for the mechanical construction of the system housing, and have EOT, Inc build it.

2.2. Purchase optical supports and cameras, and mount them inside the completed housing (2.A). Interface optical and electronic components to microcomputer, and microcomputer to x-ray generator. Write software to orchestrate both auto-calibration procedures as well as digital image acquisition.

Task 3: Measure performance of digital mammography system [months 24-36]

3.1. Measure the MTF of the system, and optimize alignment, focus and acquisition to assure maximum spatial resolution

3.2. Measure the DQE of the system. Also estimate the figure of merit, $[SNR]^2$/Dose, for a range of acquisition parameters (e.g. grid or no-grid, kV, object thickness).

3.3. Digitize film images taken under identical technique settings (kV & mAS), and compare contrast to noise ratio and spatial resolution

Task 4: Evaluate algorithms for the processing and display of the dual-energy and single energy images. [months 24-40]

4.1. Investigate potential of neural network to perform both noise suppression and dual-energy subtraction in a single pass.

4.2. Write software to allow easy, mouse-driven interaction with the image data base and with the images as they are displayed. Develop algorithms to identify calcifications on the dual energy image, colorize them, and superimpose them onto the low-energy and/or the (low + high) energy images.

Task 5: Perform a limited clinical study comparing the performance of the digital system with film-screen mammography. [months 36-48]

5.1. Recruit patients who have mammographically-identified lesions, and after receiving consent, make images of the area(s) of the breast which contain the lesions.

5.2. Make visual comparisons between the screen-film images and those acquired with the digital system. Digitize the film-screen images on a laser scanner and compare both image types in digital format. Make measurements of contrast to noise ratio on both digitized film images and on the acquired digital mammograms. Compare.

6. Body of Report

This project encompasses a very wide array of different scientific undertakings, from computer simulations to the actual design and fabrication of the mechanical, electrical, and optical components of an imaging system. We have approached this project in parallel, with a large number of sub-projects that are leading towards the ultimate goal of building and testing the performance of a dual energy digital mammography system. In setting out on each individual project, we realized that it was important to start at the basics and work up. Consequently, we have spent a great deal of effort in establishing base parameters for each sub-project, and this will become clear later. Below, a total of eight projects are described, and they may seem a bit disconnected at first glance. However, all of these sub-projects are providing the groundwork for the optimal design, construction, and testing of the dual energy mammography system. In the following description of the sub-projects, we will attempt to make it clear what the relationship the sub-project has in terms of the Statement of Work (which was provided above for reference).

As with any scientific project, some things don't go as expected and research plans are modified to accommodate new knowledge. Delays in the acquisition of key devices (CCD cameras), which were solely the responsibility of the CCD vendor (Princeton Instruments, Inc., New Jersey) have also changed the order of what we have been working on from the original Statement of Work. We also came across a new device (x-ray diffraction spectrometer), whose development was funded by an Army grant (P.I. Richard Deslattes, Ph.D., National Institute of Standards and Technology). With this device, we now have the capability of measuring x-ray spectra (rather than relying on computer-modeled spectra) and we are presently cataloging a series of x-ray spectra measurements.

Presently, we have four manuscripts which describe work funded by this grant in submission to peer reviewed journals and another to be submitted next week. These manuscripts are listed below:

1. JM Boone, Tong Yu, J.A. Seibert, Sinusoidal modulation analysis for optical system MTF measurements, submitted to Medical Physics in November 1995 (second revisions are due and manuscript is preliminarily accepted for publication upon minor corrections)

2. JM Boone and AE Chavez, Comparison of x-ray cross sections for diagnostic and therapeutic medical physics, submitted to Medical Physics in April 1996

3. T Yu, JM Sabol, JA Seibert, and JM Boone, Scintillating fiber optic screens: A comparison of MTF, light conversion efficiency, and emission angle with $Gd_2O_2S:Tb$ screens, submitted to Medical Physics in April 1996

4. T Yu and JM Boone, Lens coupling efficiency: derivation and application under differing geometrical assumptions, submitted to Medical Physics in May, 1996

5. JM Boone, KK Lindfors, CS Beatty, and JA Seibert, A breast density index (BDI) for digital mammograms based on radiologists ranking, to be submitted to Radiology, August 1996

Below is a short description of each of a series of sub-projects related to this grant:

6.1 Spectral Measurements

Tasks 1.1 and 1.2 are concerned with determining the most efficient x-ray spectrum for dual energy imaging. While we have a reasonable experience with computer simulations, it is necessary to stop along the way and provide a comparison between computer simulation data and real world measurements. We get this comment all the time from reviewers critiquing Monte Carlo simulation papers, and understandably so. We were fortunate enough to get one of Dr. Richard Deslattes' x-ray spectrometers which he has developed under Army BCRP funding at NIST, and are presently using this device to make experimental measurements of mammography spectra. While we had possession of an earlier device last year, we worked with Dr. Deslattes' research team to get a spectrometer capable of measuring lower energies. This required changing the lattice structure (different orientation and bending of the silicon wafer) of the defractometer. We just received the updated spectrometers, and are currently in the process of calibrating the x-ray spectrometer in a scientifically defensible manner. This involves getting multiple different energy sources (such as k-absorption edges and characteristic x-ray lines) to calibrate the energy bin (the x-axis of the spectrum), but more complicated is the calibration of the photons per bin (the y-axis of the spectrum), since a lot of variables are folding into this measurement.
Raw x-ray spectra measured with the Deslatte spectrometer are shown below in Figure 2.
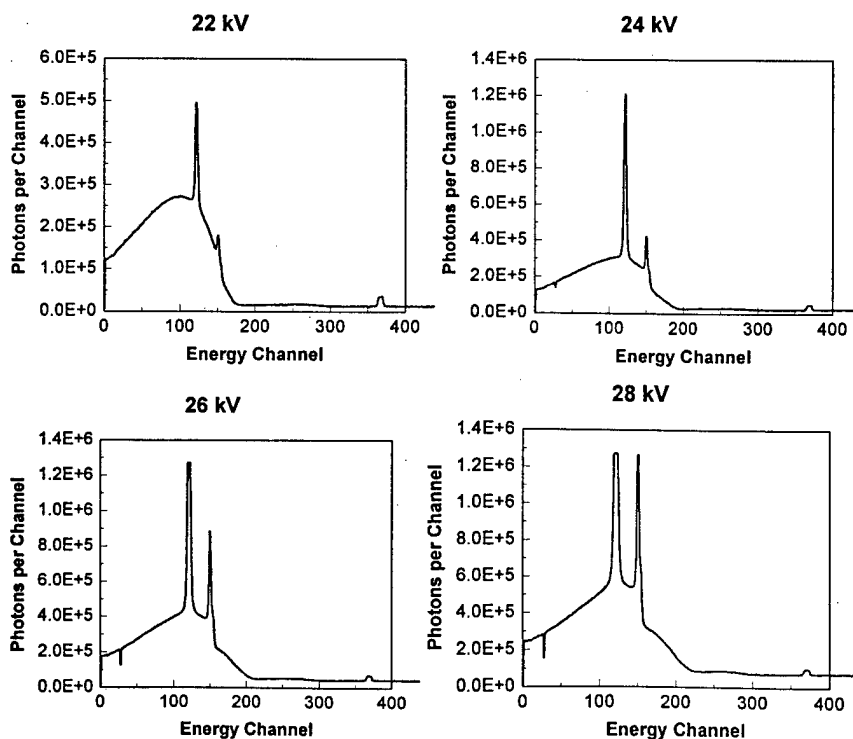
Figure 2: A series of measured spectra from the Deslattes x-ray spectrometer. The spectra shown run from 22 to 32 kV. Calibrating the Energy Channel is straight-forward using the kVs, characteristic spectra (e.g. the 17 and 19 keV emission from molybdenum) and absorption edges (not shown). These spectra were measured without any added filtration. At the higher kVs, it is apparent from the graphs that the characteristic lines were driven beyond the dynamic range of the system.

8
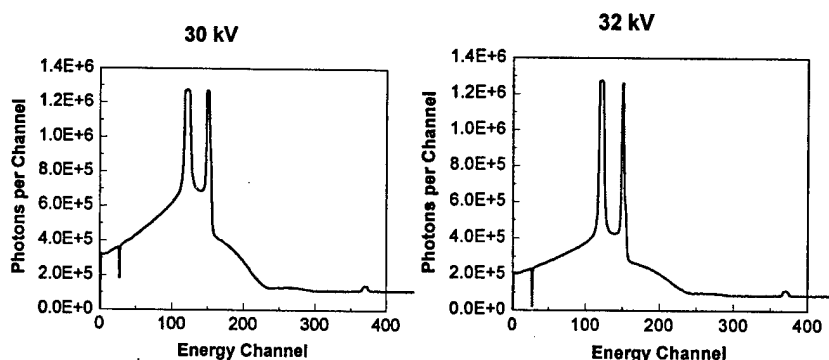
Measured spectra with various filter materials are shown in Figure 3.
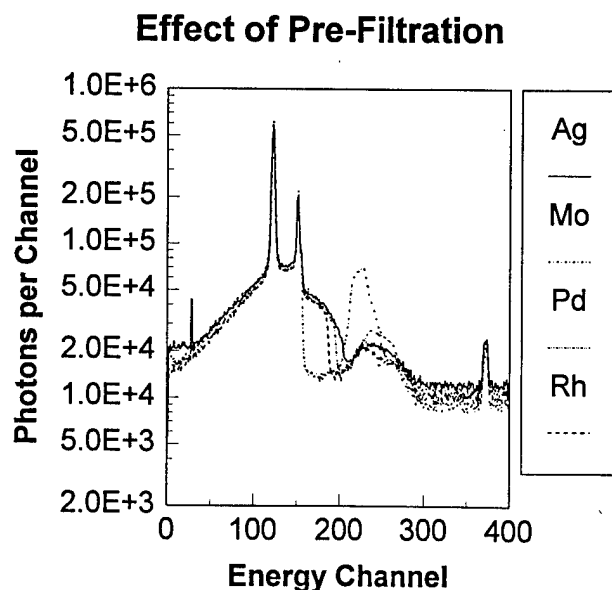
Figure 3: A 26 kV spectrum is shown filtered with four different metal foils. The addition of filters, of course, is a common way to optimize the shape of x-ray spectra to maximize signal to noise ratio and to minimize radiation dose to the patient.

The characterization of x-ray spectra is ongoing in our laboratory. The Deslattes spectrometer has an upper energy limit of about 50 keV, and thus the spectrometer may not be useful for determining spectra produced with kVs greater than 50-60. Nevertheless, we are using the device to characterize tungsten anode systems operated below 50 kV. There has been a lot of interest in using tungsten systems because of the high heat loading and better efficiency of tungsten tubes, for example in the Fischer (Yaffe) Slot/Scan digital mammography system soon to hit the pre-market approval phase.

## 6.2 Evaluation of Novel Screen Design for Dual Energy System

As mentioned in last year's annual report, we have modified the initial design of the dual energy system in a manner that should further improve the signal to noise ratio of the dual energy image. This new design scheme uses sandwhiched detectors combined with rapid (millisecond) switched kV, where the acquisition of the low and high energy signals (from CCD cameras) are sequenced in an optimum way. One of the limitations of a sandwhiched detected is that the rear (high energy) detector needs to be read-out from the back, which can lead to less resolution and less light output per absorbed x-ray photon.

9

To address this limitation, we are studying fiber optical face plates and have developed a new hybrid grid/detector system for the rear screen, and are in the process of characterizing the performance of both of these systems in the laboratory and in computer simulations.

The angular emission of light generated in a screen is very close to Lambertian, however this is not the case with a scintilating fiber optical face plate (made of scintilating glass). We have evaluated this angular dependency (Manuscript #2 listed above) and the results are presented in Figure 4.
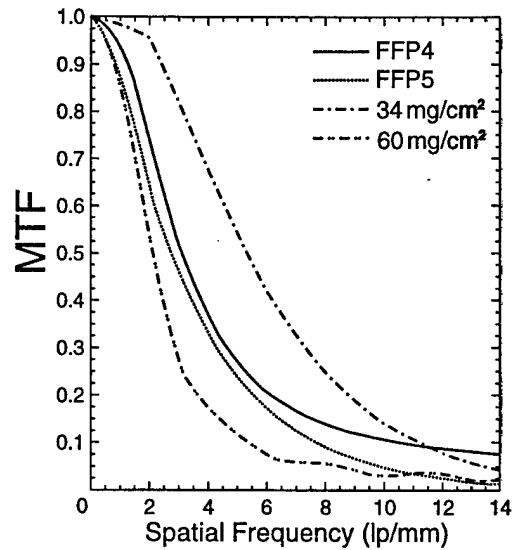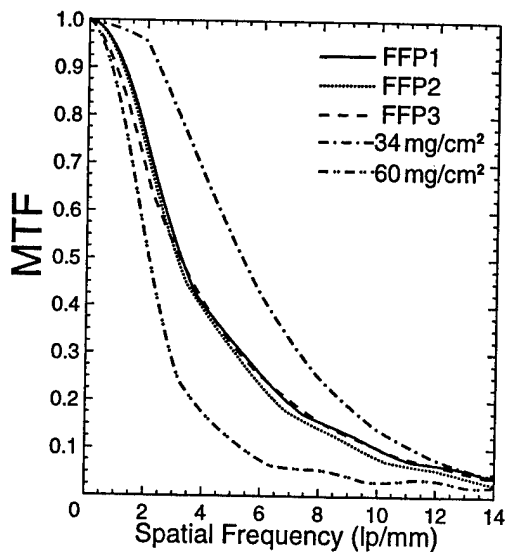
Figure 4: The MTFs of two screens, the 34 mg/cm^2 Gd$_2$O$_2$S screen is a Min-R screen, and the 60 mg/cm^2 version is a regular lanex screen. The MTFs of the screens are compared to the MTFs of 5 different fiber optical scintillating face plates (FFP). The FFPs were manufactured by Collimated Holes, Inc. in California, and were on loan to us for evaluation. It is apparent that the FFPs all have spatial resolutions (as shown by the MTFs) intermediate between the Min-R and Lanex screens.
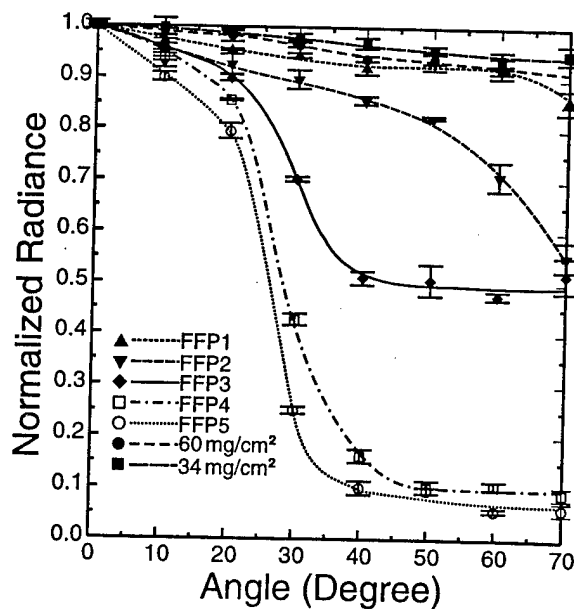

Figure 5: The light output (normalized radiance) as a function of angle, where 0° corresponds to the normal to the plane of the detector. Again, the Min-R and Lanex screens are compared to the five FFPs. The conventional screen emission is very close to being Lambertian, and that is true for some of the FFPs as well (it turns out that this is the case because some of the FFPs provided were encased in glass which caused significant light scattering). Two of the FFPs are seen to be very forward peaked in terms of light emission, and this is extremely good news in a lens coupled system as we are designing.

We are in the process of identifying the optimal design characteristics for a scintillating glass fiber face plate, and are also evaluating similar technology based on a microchannel plate.

6.3 Analytical comparison of screen efficiency (affecting DQE)

We have used the measured MTFs and the angular distributions shown above in Figures 4 and 5 in an analytical evaluation of light collection efficiency, comparing screens and fiber optical face-places. The reader will recognize that the number of light photons collected by the CCD camera, per absorbed x-ray photon in the screen, is a key parameter in the performance of the imaging system. This "gain" stage will impact to a large extent whether or not a secondary quantum sink exists. Secondary quantum sinks are undesirable, and result in a reduced detective quantum efficiency (DQE[f]). For the sake of brevity, we will not repeat the analytical derivations leading to the results. These have been submitted for publication (Manuscript #4 listed above), and will be a part of our final report to the US Army.

The results of our calculations are shown in the figures below:
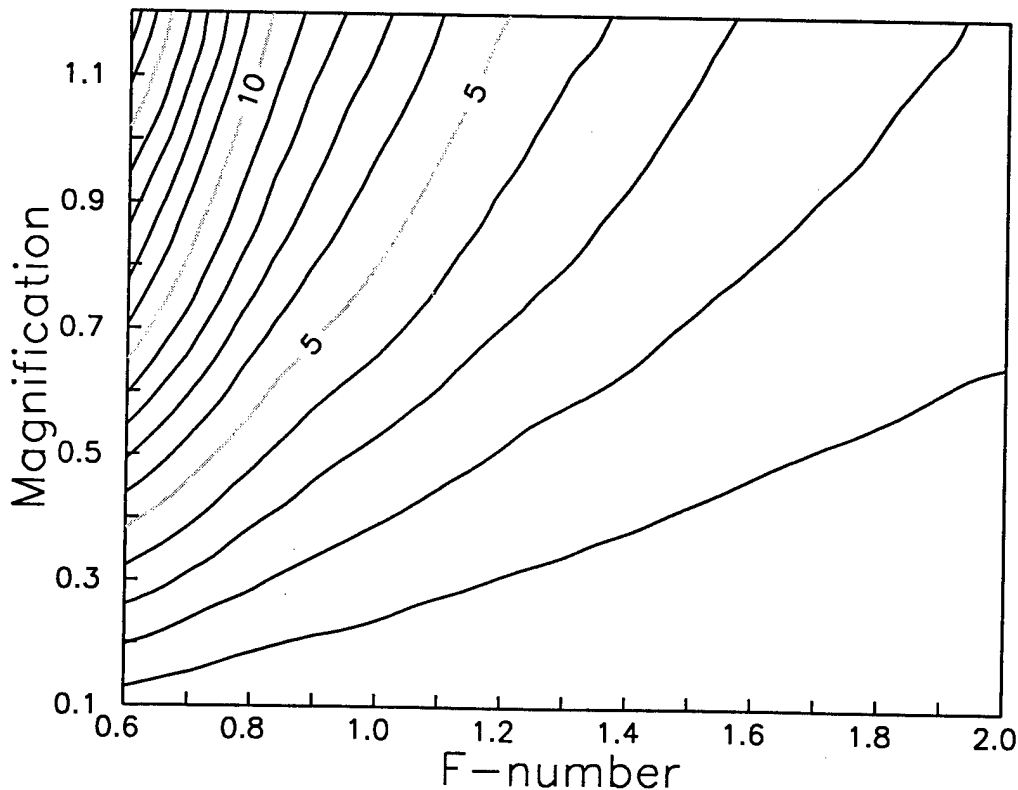
Figure 6: The number of light photons detected in a CCD camera per x-ray absorbed in the scintillator, for a Lanex 60 mg/cm^2 screen (back side). The number of collected light photons (the efficiency) increases with less magnifications (between the CCD chip and the plane of the scintillator) and of course with a faster lens (lower F-number). It is our design goal to image a 10 cm × 10 cm field of view, using a 2.5 cm × 2.5 cm CCD chip, corresponding on this figure to a magnification of 0.25. Using a F/1.2 lens, which is what we could afford in this project, for the Lanex screen only about 1 light photon per x-ray photon would be collected.

12
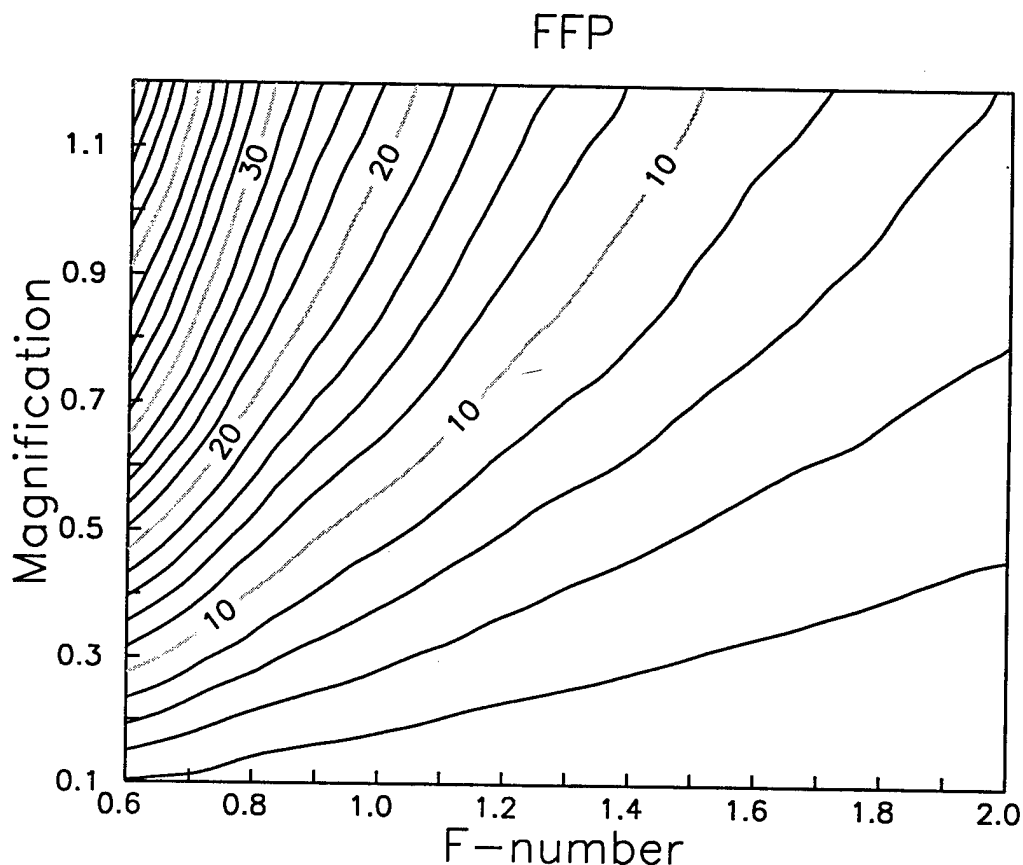
Figure 7: The number light photons per absorbed x-ray photon absorbed in a scintillating fiber optical faceplate is shown. Because of the more forward peaked (i.e. non-Lambertian) emission of the fiber optical faceplate, more of the emitted light actually reaches the lens, resulting in greater efficiency. As seen on this plot, at a magnification of 0.25 and an F-number of F/1.2, about 3 light photons are collected per absorbed x-ray.

Although the above calculations indicate that the fiber face plate is 3 times as efficient as the Lanex screen, the collection of only 3 x-ray photons per absorbed x-ray photon is still too low to eliminate a secondary quantum sink in the imaging system. While this could be increased by going to a more expensive F/0.9 lens, money is not available for this in our present budget (initial estimates for a F/0.9 lens were about $3000 each). Consequently, we are planning to reduce the field of view in order to eliminate a secondary quantum sink. We could conceivably go to a field of view of about 5 cm x 5 cm, resulting in a magnification factor of 0.5, and a collection of almost 8 light photons per absorbed x-ray photon. The smaller field of view should not be a problem in evaluating phantoms. It was the recommendation of the study section (which cut the budget by 27%) that we eliminate the clinical study, but we are still interested in imaging a few women as a feasibility study. These women will have had abnormal findings under routine screening mammography, and the area of suspicion will therefore already have been identified. Therefore, the smaller field of view should not be a problem. We will make the final decision as to whether or not we will proceed with a clinical study as the system development proceeds in this next year.

6.4 Comparison of "New" Attenuation Data

Monte Carlo calculation of photon transport is highly dependent upon the tabulated cross sections used in the program. Up until last year, we (and most medical physicists, we suspect) had been using the 27 year old McMaster attenuation coefficients combined with the 26 year old Storm and Israel mass energy coefficients. Of course attenuation coefficients do not change over time, but our understanding of them does. Because of our relationship with our sister institution, the Lawrence Livermore National Laboratory, which is administered by the University of California and is geographically close to us at U.C. Davis (about 60 miles), we were able to access their on-line updated cross section data. This data includes both mass attenuation coefficient and mass energy coefficients, which are necessary in calculating interaction probabilities and energy deposited in a Monte Carlo simulation.

We took the data which was kindly provided by colleagues at LLNL, and trimmed out values outside of the range of radiology energies and wrote computer programs for interpolation and unit conversions (from Barns to cm^2/g). The resulting single program can calculate cross sections between E=1.0 keV and 50 MeV, and from Z=1 to Z=100, inclusive. It can also yield either the mass attenuation, mass absorption, or mass energy absorption coefficients, for all interactions combined or for each individual interaction type (photoelectric, Rayleigh and Compton scattering, pair production and triplet production). Examples of the output of this program is shown below:
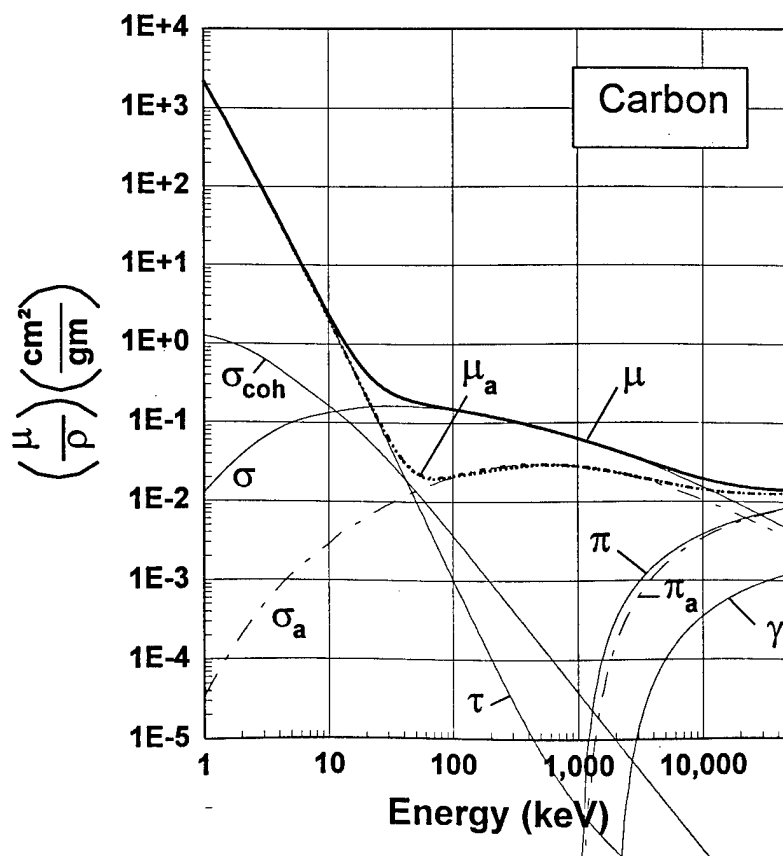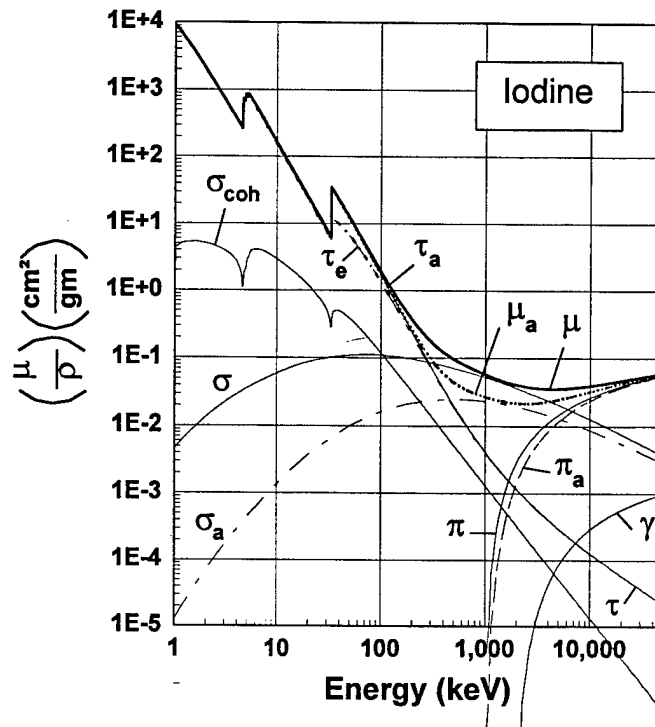

Figure 8: The cross sections for various interaction types for Carbon.
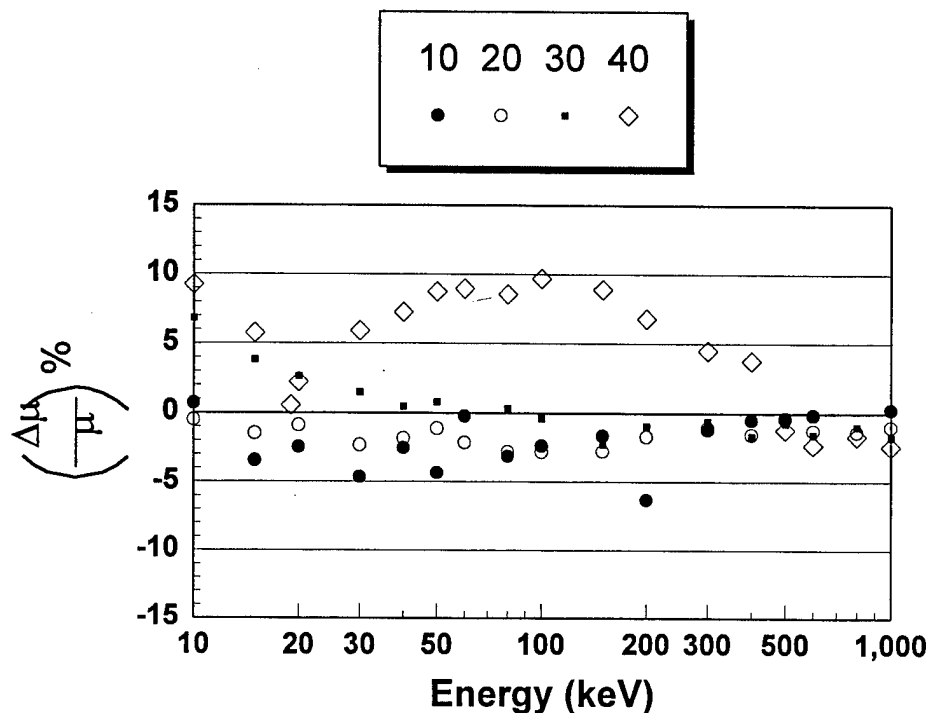
14

Figure 9: The cross sections for various interaction types for Iodine.

Before setting out blindly using the new coefficients, we felt it both necessary and a reasonable contribution to the field make comparisons between this new data set and the older cross section standards used in the field. These comparisons resulted in manuscript #2, listed above. Examples of the comparisons are shown in the figures below.
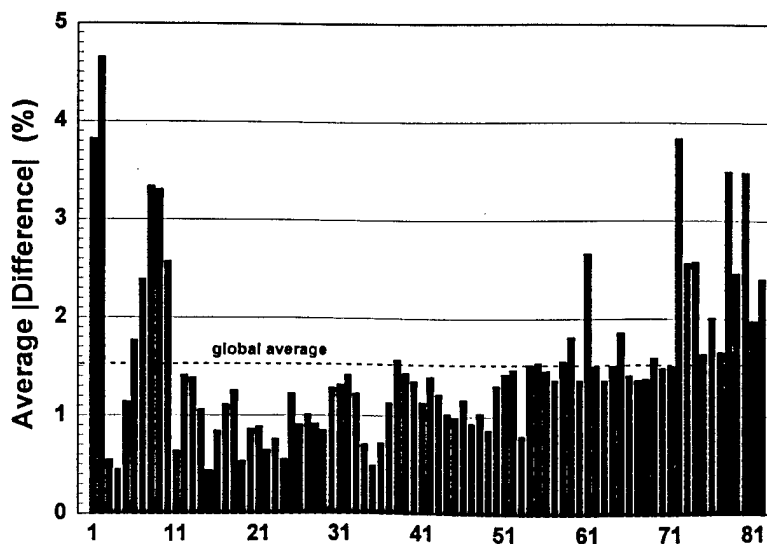
Figure 10: The overall (positive) differences (summed over the energy region between 10 keV and 1000 keV) between the 1996 LLNL data and the 1969 McMaster mass attenuation coefficients is shown.

15

10 20 30 40

● ○ ▪ ◇

15

10

5

$\left(\dfrac{\Delta\mu}{\mu}\right)$ %

0

-5

-10

-15

10 20 30 50 100 200 300 500 1,000

Energy (keV)

Figure 11: The differences between the 1996 LLNL data and the 1970 Storm and Israel mass energy coefficients is shown.

Figures 10 and 11 are representative of the comparisons made between the new and existing attenuation data; a comprehensive analysis was included in the submitted manuscript. With the characterization of the new cross sections, we are now incorporating these new values into our Monte Carlo code, and will be finishing Tasks 1.3 and 1.4 in the next few months.

6.5 Development of a sine-wave test pattern technique for MTF evaluation

Because of the delays in receiving the CCD cameras which we ordered last November from Princeton Instruments (we just received them last week), we were not able to complete the assembly of the digital imaging system at this time, however this task will be finished by the November time frame. Therefore, we forged ahead and developed some of the computer programs required for evaluating the performance of the digital imaging system (Task 3).

The most common method for measuring the MTF is to image a slit, compute the line spread function and then apply the Fourier transform to compute the OTF and then the MTF is calculated. In x-ray imaging, direct measurement of sinusoidal modulation has never been feasible because of the complexity of building a test phantom which would modulate a polyenergetic x-ray beam in a sinusoidal manner. However, for the optical components of the digital imaging system that we are developing, optical sinusoidal patterns are available. We set out to develop a methodology in which we could incorporate a sine pattern into our evaluation of system resolution, and this has lead to manuscript #1,

listed above. Images of the sine patterns were produced using our CCD cameras, and software was written to fit the sinusoidal gray scale data. Some examples of these fits are shown below.
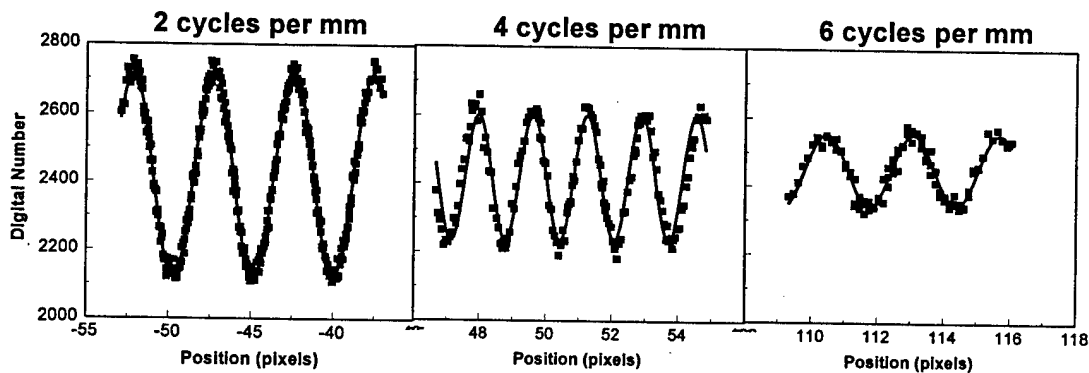
Figure 12: Three different spatial frequencies are shown, with the measured gray scale values shown as solid squares and the best fit sine curve is shown as a line.

The output modulation of the sinusoid $\{(G_{max}-G_{min})/(G_{max}+G_{min})\}$ can be calculated from the fit coefficients of the sine function (solid lines in Figure 12). The input modulation at each frequency is known, as it was supplied by the manufacturer of the sine pattern (Sine Patterns, Inc.). The MTF is then calculated as the ratio of the output modulation to that of the input modulation, at each spatial frequency measured.

This procedure was used and compared against the Fujuta method[8] which is the standard used in digital radiography. These results are shown below:
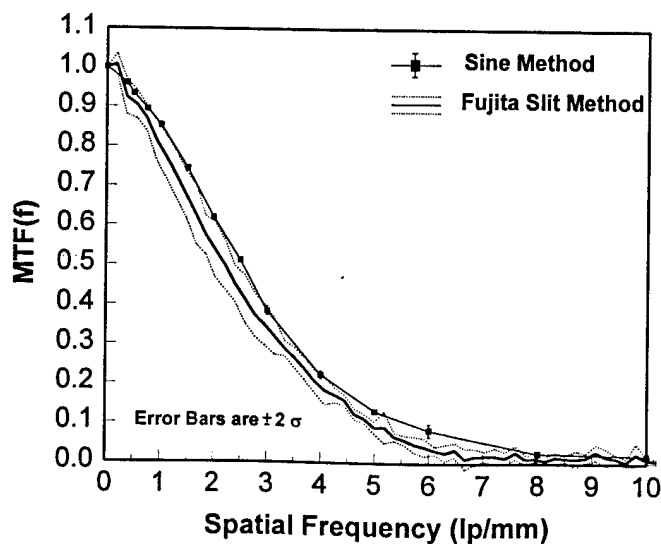
Figure 13: The MTFs determined from the Fujita method and by using the sinusoidal method discussed above. The methods compare well with each other.

We hope to utilize this methodology for determining the MTF into the automatic focusing procedure for the CCD cameras.

## 6.6 Development of alignment procedure for registering dual energy images.

Task 2.2 required the development of computer programs for the auto calibration and computerized registration between the high and low energy images. These routines have been developed, and the computer registration algorithm and its performance is described below.

In single-pulse dual-energy digital imaging systems, two cameras are employed. Since the two cameras have different artifacts and distortions, the two acquired images have different orientations, magnifications, and aberrations. These differences are dependent on the system setup. Once the system setup is finalized, the differences are fixed. Therefore, the spatial alignment calibration procedure needs to be done only occasionally. A phantom with an array of BB's was used as a calibration tool to get two sets of data for two CCD cameras. An interactive program was written to locate the BB's position. The region of interest (ROI) containing the BB was chosen, and the histogram of the ROI was calculated and displayed. From the histogram the threshold value was selected and pixel values that fell below the threshold were set to zero, and pixel values that were greater than the threshold were set to 4095. The coordinates of the BB were then determined using center of mass equations, which allowed the determination of BB locations at non-integer points on the imaging matrices.

Once two sets of BB coordinates from the two images are obtained, any image pair obtained by these two cameras can be aligned using the following warping algorithm. One image was chosen to be "correct" and the other was then considered to be distorted, and then the distorted image is warped to match to the "correct" image. The images were partitioned into multiple triangular regions, each bounded by three BB coordinates. The following transformation was developed for each triangular region:

$$
\begin{aligned}
x_1' &= \alpha_x x_1 + \beta_x y_1 + \varepsilon_x, \\
x_2' &= \alpha_x x_2 + \beta_x y_2 + \varepsilon_x, \\
x_3' &= \alpha_x x_3 + \beta_x y_3 + \varepsilon_x, \\
y_1' &= \alpha_y x_1 + \beta_y y_1 + \varepsilon_y, \\
y_2' &= \alpha_y x_2 + \beta_y y_2 + \varepsilon_y, \\
y_3' &= \alpha_y x_3 + \beta_y y_3 + \varepsilon_y,
\end{aligned}
\tag{1}
$$

Where (x_1, y_1), (x_2, y_2), and (x_3, y_3) are three BB coordinates of the correct image, and (x_1', y_1'), (x_2', y_2'), and (x_3', y_3') are the corresponding coordinates of the distorted image. The values for α_x, β_x, ε_x, and α_y, β_y, ε_y were determined algebraically from the 3 pairs of known BB locations, and the coefficients were used to transform the pixels within each triangular region. Two dimensional linear interpolation was used to map gray scale values at each position (x', y') in distorted image to position (x, y) in new corrected image for each triangular region. The before and after results of the image warping are illustrated in Figure 14 and Figure 15.
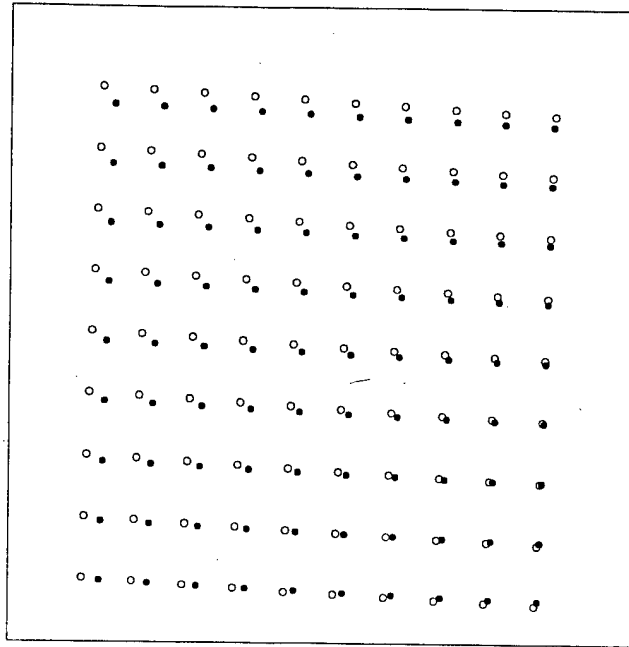
Figure 14: The BB locations from the two unregistered images are shown. The solid circles correspond to the "correct" image, and the open circles are the BB locations on the image to be warped.
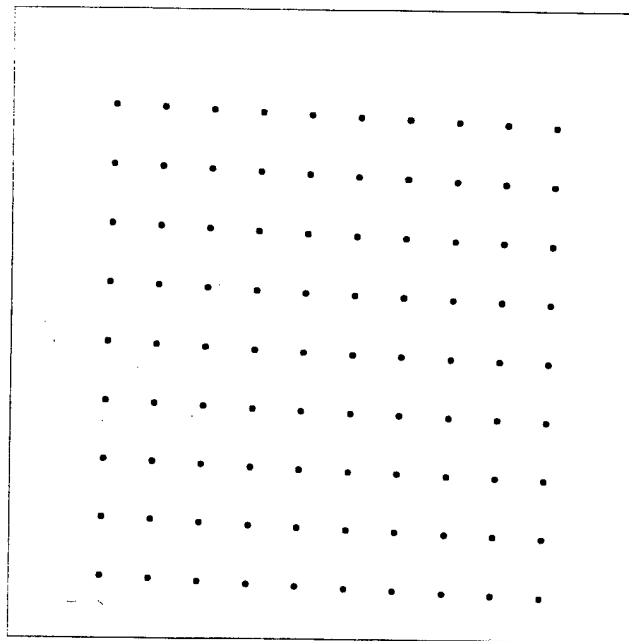

Figure 15: After the warping procedure has been performed, the BB's are shown to overlap. The open circles are plotted here, they are however not visible because of their precise alignment with the solid circles. ·

6.7 Development of a Breast Density Index (BDI) for quantitative characterization of breast density

One of the principal advantages that dual energy mammography may offer over single energy mammography is the (hopefully) improved ability to image the dense breast, as was discussed in the Introduction. While not explicitly listed in the Statement of Work, it was clear to us that a quantitative index relating to breast density needed to be developed. We have spend considerable effort in developing a quantitative index which follows the subjective but amazingly reproducible rating of an experienced mammographer in terms of the assessment of breast density.

The computer calculation of the Breast Density Index is derived from six features calculated from digitized mammograms. A data set of 160 pair of mammograms (CC and MLO images) was used for the development of the BDI. The images were digitized using a laser digitizer (12 bit), and corrections were made to produce images that are linear with μx to the extent possible. This was done by linearizing the digitized film images using a look up table to correct for the H and D curve of the film, and then in areas outside of the breast image an estimate of the I_0 was made. Inside the region of the image defined by the breast, the digital numbers are related by $I_0 \ e^{-\mu x}$. Straightforward algebraic manipulation of these equations leads to a digital mammogram linear with μx. After searching hundreds of parameters for good predictors of breast density as determined by the ranking of the mammographer, six parameters were selected. These parameters were used in a multiple linear regression analysis to calculate the breast density index on a scale form 0 (least dense) to 100 (most dense). A manuscript on this topic has been written, and will be submitted next week. Some of the results of this research are shown below:
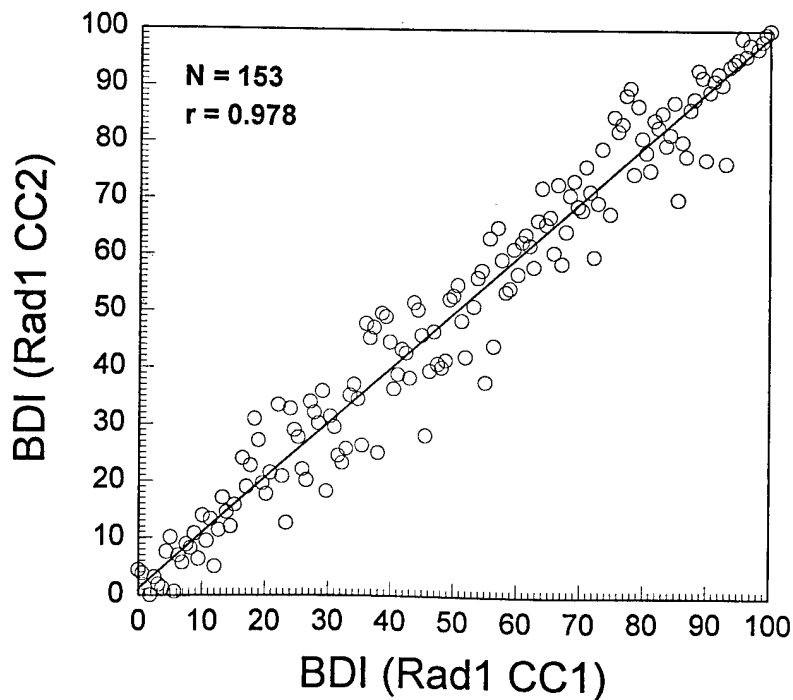
Figure 16: This figure shows the correspondence (image by image) between two rank orderings performed by the mammographer (co-investigator on this grant, Karen Lindfors, M.D.). A surprising level of reproducibility was found.
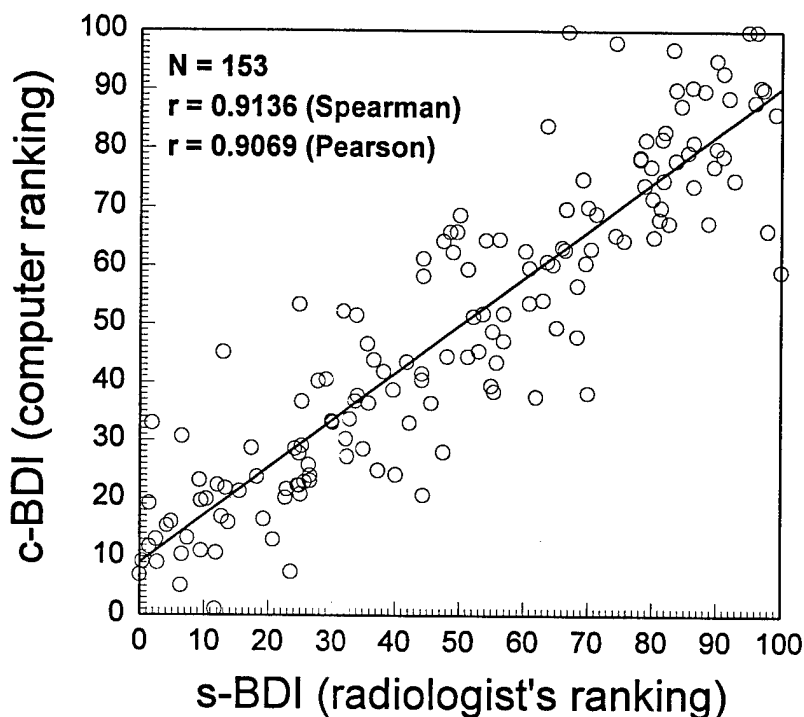
Figure 17: This figure shows the correspondence (image by image) between the radiologist's rank ordering and the computer's determination. These data are test data, resulting from an independent determination of the multiple regression coefficients from a jackknifed training set. The computer determined Breast Density Index (BDI) is a good predictor of breast density, and is related to the radiologist's notion of a dense breast.

The quantitative evaluation of breast density will enable us to determine the anticipated improvement of dual energy over single energy digital mammography, *as a function of breast density*. We anticipate that the improvement factor (dual energy over single energy performance) will increase with increasing breast density. With the development of the BDI, we now have a computerized technique to assign quantitative estimates of breast density.

6.8 Mechanical fabrication of the digital mammography system.

The mechanical fabrication of the system has gone from the drawing board (presented in last year's annual report) to reality. A large set of linear struts have been acquired, in 12", 24", 36", 48" and 96" lengths, and are presently in our laboratory. The struts were machined from 1" × 1" channel aluminum, drilled out every inch with 1/4-20 holes, and black anodized. They mesh well with the optical tables which serve as the base of the digital mammography system. A picture of the system is shown in Figure 18. The stepping motors which control the position and focus of the CCD cameras have been successfully interfaced to the controller (a Pentium computer).
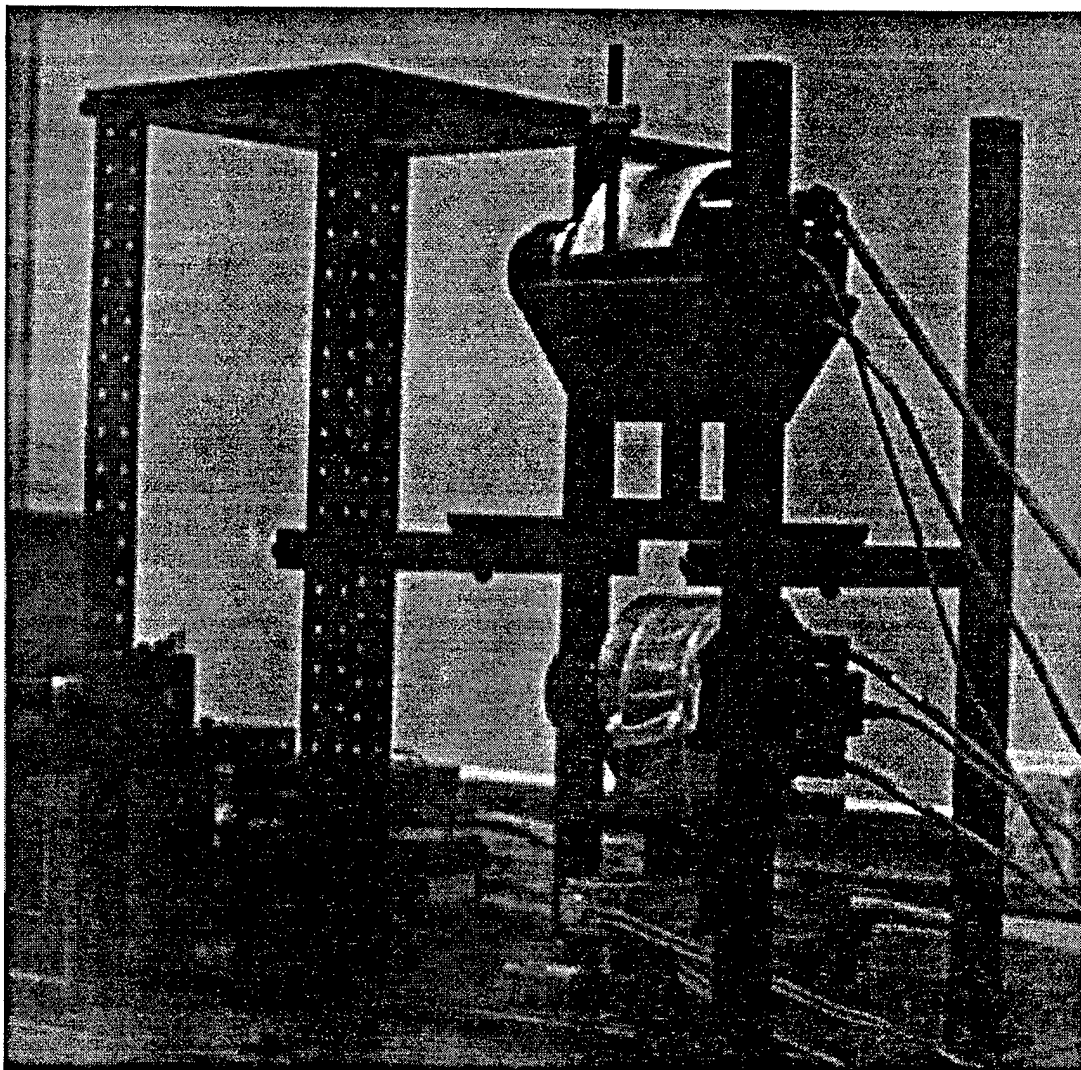
Figure 18: An image of the system setup presently in the laboratory. The anodized struts allow the flexibility to build the mechanical support of the electronics, mirrors, and screens in any configuration we desire. Upright supports are shown here, with 2 CCD cameras. The stepping motor for moving the lower camera laterally is also visible.

Figure 18 just shows the strut system we have for fabrication of the mechanical housing of the digital mammography system, it is not meant to illustrate a digital mammography system per se. We are awaiting a carbon fiber plate which will serve as the imaging surface for the system, which we expect to receive within the month. Since we just received our new 2k × 2k CCD cameras, we are in the process of deciphering the software that was written to our specifications. Once the carbon fiber plate is received and we have figured out how to run the cameras, we will have the dual energy digital mammography system assembled and operational. We hope that this will occur on the November '96 time frame.

7. Conclusions

The development of the dual energy digital mammography has proceeded well over the past year. We have chosen to start at some very basic levels in our development of the software and hardware, and this has given us some better insight and better confidence that we are proceeding in a logical and scientifically prudent manner. Our progress has been nominal, meaning that we are just about where we need to be in terms of the development of the research plan. We have some components of the research done ahead of schedule, and about an equal number of things behind schedule. In the course of the last two years of research, we have responded to new ideas by modifying and improving the design goals of the dual energy mammography system.

In this report we have presented a snapshot of several loosely related projects, all addressing our development of the dual energy system at a different point of focus. Our goal for the next year is to integrate these parallel projects towards a cohesive and concentrated effort on producing a high quality dual energy x-ray system. We remain excited about the prospects of dual energy mammography, and look forward to the next 12 months of development of the system with vigor and enthusiasm.

8. References

1. F. Shtern, "Digital mammography and related technologies: a perspective from the National Cancer Institute," Radiology.**183,** 629-630 (1992)

2. H.P. Chan, K. Doi, C.J. Vyborny et al."Improvement in radiologists' detection of clustered microcalcifications on mammograms. The potential of computer-aided diagnosis," Invest. Radiol.**25,** 1102-1110 (1990)

3. H. Chan, K. Doi, S. Galhotra, C. Vyborny, H. MacMahon, and P. Jokich, "Image feature analysis and computer aided diagnosis in digital radiography: 1. Automated detection of microcalcifications in mammography," Med. Phys.**14,** 538 (1988)

4. D. Davies, D. Dance, and C. Jones, SPIE.**1092,** 153 (1989)

5. F. Yin, M. Giger, K. Doi, C. Metz, C. Vyborny, and R. Schmidt, "Computerized detection of masses in digital mammograms: Analysis of bilateral subtraction images," Med. Phys.**18,** 955 (1991)

6. C.B. Caldwell, S.J. Stapleton, D.W. Holdsworth et al."Characterisation of mammographic parenchymal pattern by fractal dimension," Phys. Med. Biol.**35,** 235-247 (1990)

7. M. Giger, "Computer aided diagnosis in digital mammography (Abstract)," Med. Phys.**19,** 864 (1992)

8. H. Fujita, D. Tsia, T. Itoh et al."A simple method for determining the modulation transfer function in digital radiography," IEEE Transactions on Medical Imaging.**11,** 34-39 (1992)